

THE CHARGE STRUCTURE OF MULTIPARTICLE FINAL STATES IN pp
COLLISIONS AT 102 and 400 GeV/c*

C. Bromberg, D. Chaney, T. Ferbel, T. Jensen, R. Schindler,
P. Slattery and D. Weingarten
University of Rochester
Rochester, N.Y. 14627

and

A. A. Seidl and J. C. VanderVelde
University of Michigan
Ann Arbor, Mich. 48104

February 17, 1975

Abstract

We investigate the distribution of charge in events produced by pp collisions at 102 and 400 GeV/c. The data are from exposures of the FNAL 30-inch bubble chamber. A comparison of the energy dependence of the data with Monte-Carlo simulations of random charge distributions provides support for the hypothesis of local compensation of charge. Results on charge transfer are in qualitative agreement with predictions of an independent cluster emission model.

Submitted to Phys. Rev. for publication.

*Supported in part by the U. S. Atomic Energy Commission.(Contract No. AT(11-1)-3065

Individual copies will be supplied as long as supply lasts.

I. Introduction

A detailed investigation of the charge structure of many-particle events has been proposed as a source of useful information concerning the underlying mechanism of particle production⁽¹⁻⁶⁾. In particular, the behavior of the charge transfer, u , (defined for pp collisions as one half the difference between the charge in the forward and backward hemispheres of the center-of-mass system) has been examined to test fragmentation models⁽¹⁾ and multiperipheral models^(2,3) of particle production. A discussion of inclusive and semi-inclusive properties of u will be given in the third section of this paper. In the remainder of the introduction, and in Section 2, we will adopt the formalism of Krzywicki and Weingarten to look for evidence of a suggested "local compensation of charge in rapidity space" (LCC)^(4-6,8).

The charge structure of an event with N charged particles in the final state can be characterized by a zone graph:

$$Z(y) = \sum_{i=1}^N q_i \theta(y-y_i) - q_{\text{beam}} \theta(y-y_{\text{beam}}) - q_{\text{target}} \theta(y-y_{\text{target}}) \quad (1)$$

where q_i is the charge of the particle i , $\theta(y-y_i)$ is the usual step function given by 0 for negative arguments and 1 elsewhere, and Z may be regarded as a generalized charge transfer across the rapidity value y . (Zone graphs are illustrated in Fig. 1.) Regions of y over which $Z(y)$ remains positive (negative) are called zones of positive (negative) polarity; gaps of no charge transfer ($Z=0$) separate each successive pair of zones. A distinction will be made between "end" zones containing either beam or target particles ("compensating" charges) and "central" zones containing only final-state particles.

The LCC hypothesis, in one formulation, requires that for sufficiently large values of the energy in the center-of-mass system (\sqrt{s}):

- (1) The internal structure of zones, partially specified for example by the mean zone length $\langle \lambda_z \rangle$ and the mean number of charges per zone $\langle n_z \rangle$, becomes independent of s .
- (2) Correlations between pairs of zones decrease quickly with increasing separation in rapidity space.
- (3) The mean number of zones, $\langle N_z \rangle$, grows with energy as $\ln s$ ⁽⁴⁾.

Although these conditions are similar to the short range order (SRO) hypothesis, a distinction exists in that a collection of events including diffractive production channels would not fulfill SRO but might, nonetheless, exhibit local compensation of charge.

In Section II, to assess the degree of validity of the LCC hypothesis, we will compare the charge structure of the measured events with the charge structure of a set of fictitious events obtained by randomly reassigning charges to the observed particle tracks. The characteristics of this "randomized charge model" (RCM), which conserves total charge but randomizes the charge distribution of the experimental data, will be used whenever simple theoretical expressions for random behavior are unavailable.

The data to be presented are from approximately 3000 measurements of inelastic pp collisions at 102 GeV/c and from 2200 measurements of collisions at 400 GeV/c. The events were observed in exposures of the FNAL 30-inch bubble chamber to extracted proton beams of machine energy. The experimental procedures at 102 GeV/c are described in previously published work ⁽⁷⁾. Similar analysis procedures were employed for the data at 400 GeV/c. The major source of systematic error is the lack of particle-identification information for particles having laboratory

momenta in excess of 1.2 GeV/c. (This region of uncertainty corresponds to $x = p_{\ell}^*/p_{\max}^* \geq -0.5$ for protons, where p_{ℓ}^* and p_{\max}^* are the center of mass values for the longitudinal momentum of the final-state particle and the incident momentum, respectively.) For a given measured momentum, the value of a particle's rapidity is affected by the choice of mass hypothesis; in particular, a pion mass assignment for high-momentum protons causes, typically, an upward shift of ~ 0.7 in rapidity. The cross section for pion production at large $|x_{\pi}|$ is small compared to that for proton production, and this fact permits us to assign, with great assurance, the proton mass to all positively charged tracks which yield reconstructed values of x_{π} greater than 0.6. This procedure diminishes somewhat the uncertainty in y due to proton/pion mass ambiguity for $y \geq 1.5$. For $|y| < 1.5$ pion production greatly dominates proton production and the bias is consequently small⁽⁹⁾.

II. Local Compensation of Charge and Zone Structure

Zone graphs for typical events at 102 GeV/c and 400 GeV/c are shown in Fig. 1. Each of the events shown contains two end zones and two central zones. The probability for observing an event containing a total of N_z zones is shown in Fig. 2. The probability distribution at 400 GeV/c is clearly shifted toward higher values of N_z . In Table I we list the means and dispersions of these distributions; we also provide these quantities calculated using our model (RCM). The data at both energies contain more zones per event than is found using the RCM. The data also indicate a faster growth of the mean number of zones with increasing incident momentum than is provided by the RCM; the ratio of the mean number of zones for the two energies $\langle N_z \rangle_{400} / \langle N_z \rangle_{102}$ is

$1.24 \pm .01$ in the data and 1.15 in the model. This rate of growth of $\langle N_z \rangle$ is somewhat smaller than the increase observed in the mean charged particle multiplicity ($\langle n_c \rangle = 6.32 \pm 0.08$ and 8.96 ± 0.10 at 102 GeV/c and 400 GeV/c respectively⁽¹⁰⁾). Dividing the mean charged particle multiplicity, increased by two units of charge (corresponding to the beam and target "compensating" charges), by $\langle N_z \rangle$, one obtains the mean number of charges per zone $\langle n_z \rangle = \frac{\langle n_c \rangle + 2}{\langle N_z \rangle}$; this quantity increases with s , indicating that the average internal structure of zones changes somewhat between our two energies. It should be noted, however, that the increase in $\langle n_z \rangle$ is smaller than expected on the basis of the RCM (see Table I).

We investigate further the internal structure of zones by examining the probability distribution of zone lengths (λ_z) displayed in Fig. 3; the relevant zone parameters are given in Tables I and II. As was the case for $\langle n_z \rangle$, the mean length of zones in rapidity, $\langle \lambda_z \rangle$, also increases with increasing s at a rate far smaller than expected on the basis of the RCM model (see Table I). Thus it appears these zone parameters reflect the presence of local compensation of charge. The data in Fig. 3 have been separated into end zones and central zones. The fact that the length distributions of these two types of zones are dissimilar may be attributed almost totally to the inclusion of the beam and target rapidities in the definition of $Z(y)$ given in Eq. (1). It is somewhat surprising, however, that the average number of charges ($\langle n_z \rangle$) for the end zones does not differ substantially from that found for the central zones. This observation suggests a similar production mechanism for the two types of zones.

Examining the behavior of the central zones, we find that there is essentially no energy dependence observed for the average central-zone length $\langle \lambda_z \rangle$. The increase in $\langle \lambda_z \rangle$ between 102 and 400 GeV/c is only $(1 \pm 1)\%$, while a growth of 7% would be expected on the basis of our RCM model. Thus, it would appear to be justified to take $\langle \lambda_z \rangle \approx 0.75$ as the value over which charge is locally compensated in the central region. Although the value of $\langle \lambda_z \rangle$ is remarkably stable, we note that $\langle n_z \rangle$ changes by $(10 \pm 2)\%$.

For completeness, we display in Table III the semi-inclusive zone parameters at 102 and 400 GeV/c. We note that the stability observed for the inclusive central values of $\langle \lambda_z \rangle$ is not maintained in the semi-inclusive channels.

Using the generalized charge transfer $Z(y)$ let us now define a zone correlation function:⁽⁵⁾

$$D(y_1, y_2) = \langle Z(y_1)Z(y_2) \rangle - \langle Z(y_1) \rangle \langle Z(y_2) \rangle \quad (2)$$

which⁽¹¹⁾, when evaluated for pp collisions at $y_1=y_2=0$, yields the variance of the charge transfer across $y=0$:

$$\begin{aligned} D(0,0) &= \langle Z(0) Z(0) \rangle - \langle Z(0) \rangle \langle Z(0) \rangle \\ &\equiv \langle u^2 \rangle - \langle u \rangle^2 = \langle u^2 \rangle \end{aligned} \quad (3)$$

Thus for $\Delta y = y_2 - y_1 = 0$, D measures the fluctuations in the charge transferred across $y = y_1 = y_2$. For intermediate values of Δy ($|\Delta y| \lesssim \langle \lambda_z \rangle$) D reflects primarily the internal structure of individual zones; and for large $|\Delta y|$, ($|\Delta y| \gg \langle \lambda_z \rangle$), $D(y_1, y_2)$ may be thought of as a gauge of long range correlations between pairs of zones.

In Fig. 4 we plot $D(y_1, y_2)$, evaluated at $y_1=0$, and -1.2 , as a function of Δy ; curves representing the results of the RCM model are given for the same y values. The data have smaller values of D than provided by the RCM curves; the discrepancy is more pronounced at the higher energy. (This implies that the high-multiplicity events do not exhibit the large fluctuations in charge transfer generated by the RCM.) The values of $D(0,0)$ are $0.90 \pm .04$ and $1.12 \pm .05$ at 102 and 400 GeV/c respectively. The small magnitude and the energy dependence of $D(0,0)$, which will be discussed later in terms of a cluster model, are cited here as further evidence for the presence of an LCC mechanism. We also note the rapid, nearly exponential fall of $D(y_1, y_2)$ as a function of Δy . This exponential behavior again indicates a strong tendency for charge transfer to occur only over small distances in rapidity space, and can be characterized by a correlation length (L) ($D(\Delta y) \sim e^{-\Delta y/L}$; with $L = 1.1-1.2$). This characteristic length is somewhat greater than the value of the average zone length $\langle \lambda_z \rangle \approx 0.75$. The exponential decrease of D for large Δy also implies a lack of significant long-range correlations between zones.

It is probably useful to point out that the well known "leading particle effect", which in LCC language is compensation of the charge of incident particles near the edges of rapidity space, cannot explain the main features of the discrepancy between the data and the RCM. For example, fixing the rapidities of the extreme positive particles and, randomizing the charges only of the remaining particles reduces the RCM values of $D(0,0)$ by ≈ 0.5 .⁽¹²⁾ The new values, 1.08 and 1.74 at 102 and 400 GeV respectively, are still significantly above the data and rise with energy more rapidly.

In the above analysis we have found that the zone parametrization yields certain regularities in the charge structure of multiparticle final states which support the LCC hypothesis. When compared to the RCM predictions, the very weak energy dependence of the mean zone length $\langle \lambda_z \rangle$ and the rapid decrease of the zone correlation function $D(y_1, y_2)$ with increasing rapidity difference Δy , are trends in the direction required by LCC. However, we also find that the mean number of charges per zone $\langle n_z \rangle$ and the magnitude of the zone correlation function $D(0,0) \equiv \langle u^2 \rangle$ rise with increasing s . These energy variations can be attributed, at least in part, to the growth of the single particle densities in the FNAL energy range. Because the latter feature of the data is ignored in the asymptotic forms of both simple multiperipheral cluster models as well as the LCC hypotheses, we anticipate that simple cluster models will also fail to provide a complete account of the observed energy variations of charge distributions.

III Charge Transfers Across $y=0$

The independent neutral-cluster emission model is one of a large class of models which satisfy the LCC hypothesis. In this section we compare the data for charge transfer across $y=0$ with a cluster model of this sort investigated by Quigg and Thomas⁽²⁾. The model assumes multiperipheral production of neutral clusters which subsequently decay into a fixed number of pions; the decay pions are dispersed over a finite region of rapidity space. The authors prove the following results for the functional dependences of charge-transfer parameters in their model:

$$\langle u^2 \rangle = \frac{K}{Y} \langle N \rangle \quad (4a)$$

$$\langle u_{\ell^-, r^-} \rangle = \frac{K}{Y} (\ell^- - r^-) \quad (4b)$$

$$\langle u_{\ell^-, r^-}^2 \rangle - \langle u_{\ell^-, r^-} \rangle^2 = \frac{K}{Y} \left[1 - \frac{K}{Y} \right] (\ell^- + r^-) \quad (4c)$$

The notation is as follows: Y is the total range of rapidities; $\langle N \rangle$ is the mean number of clusters; ℓ^- and r^- are respectively the number of negative particles emitted into the left, and right (backward and forward) center-of-mass hemispheres; K is a constant which depends only on the nature of the cluster decay. The value of $\langle N \rangle$ is assumed to grow logarithmically with s (i.e., a constant cluster density, $\langle N \rangle / Y$, is assumed), consequently the value of $\langle u^2 \rangle$ is expected to approach a constant at high energies. (Note that $\langle u^2 \rangle$ contains an averaging over all events, while the subscripted u -variables are averages over fixed multiplicity.) The magnitude of $\langle u^2 \rangle$ has already been shown to differ significantly from that expected for a random charge distribution; and here we note that the energy dependence of $\langle u^2 \rangle$, given in Fig. 5, does not yet suggest an approach to a constant value⁽¹³⁾. Since, as we have already mentioned, there is no evidence at the energies we are considering for an s -independent rapidity plateau, which is assumed in the model of Quigg and Thomas, a slow increase in $\langle u^2 \rangle$ is not surprising. (The single particle invariant cross-sections at $y=0$, integrated over transverse momenta, are 48.3 ± 2.5 mb and 64.6 ± 3.2 mb at 102 and 400 GeV/c respectively.)

Charge-transfer properties as a function of charged-prong multiplicity are given in Table IV and in Figs. 6 and 7. In obtaining these data we have made use of the symmetry about $y=0$ expected for pp collisions.

For example, in the eight-pronged topology the value of $\langle u_{2,1} \rangle$ has been averaged with $-\langle u_{1,2} \rangle$. This folding procedure tends to reduce the systematic biases in the data due to proton/pion misidentification near $y=0$. We have not corrected the symmetric entries in Table IV (e.g., $\langle u_{1,1} \rangle$) for this known bias, and consequently the deviations from $\langle u_{m,m} \rangle = 0$ provide a measure of the systematic uncertainties in our measurements. (The errors given in Table IV are statistical.)

In Figs. 6(a) and (b) we present the dependence of $\langle u_{\ell^-, r^-} \rangle$ on $(\ell^- - r^-)$ and the dependence of $\langle u_{\ell^-, r^-}^2 \rangle - \langle u_{\ell^-, r^-} \rangle^2$ on $(\ell^- + r^-)$. The straight lines given in Fig. 6 are expectations based on the independent emission (IEM) of single pions rather than pion clusters.^(1,2) The s -independent expressions in the IEM are: $\langle u_{\ell^-, r^-} \rangle = \frac{1}{2} (\ell^- - r^-)$, and $\langle u_{\ell^-, r^-}^2 \rangle - \langle u_{\ell^-, r^-} \rangle^2 = \frac{1}{4} (\ell^- + r^-)$; these simple forms are very close to the RCM values with the "leading particle effect" removed.

The data in Fig. 6(a) lie below the IEM prediction, indicating the presence of substantial clustering. The linear dependence predicted by the cluster model (Eq. 4b) is consistent with the data, however, the significant scatter in $\langle u_{\ell^-, r^-} \rangle$ at fixed $(\ell^- - r^-)$ and fixed s cannot be understood on the basis of the simple model of Ref. (2).

In Fig. 6(b) we again note discrepancies between predictions of IEM and the data. In particular, for $n_- = \ell^- + r^- < 3$ the data are above the curve, indicating the presence of diffractive "spill-over" contributions near $y=0$ ⁽¹⁾. For $n_- > 3$ the data are statistically poor, nevertheless they clearly lie below the IEM line, suggesting the presence of clustering effects (Eq. 4c).

We investigate the energy dependence of $\langle u_{\ell^-, r^-} \rangle$ in Fig. 7 where the low energy MSU data⁽¹⁴⁾ and the data at 102 and 400 GeV/c for $r^- = 0$

are plotted. The s -dependence is consistent with a $1/\ln s$ form (Eq. 4b) and extrapolates reasonably to $\langle u_{\ell^-, r^-} \rangle = 0$ for all available data.

Although parameters relating to cluster properties can be extracted from the data presented in this paper (e.g., an average of 2-2.5 charged particles per cluster), the precise values obtained for these parameters are sensitive to model dependent corrections resulting from the non-asymptotic energies of FNAL.

IV Summary

We have presented new results on the charge structure of final states observed in pp collisions at 102 and 400 GeV/c. We find significant deviations from the assumption of a random charge distribution in *inelastic final states*; this supports a production mechanism exhibiting *local compensation of charge (LCC)* at high energies. Simple cluster models, although correct in spirit, do not provide detailed agreement with the data. It appears that this lack of agreement can in part be attributed to the non-asymptotic nature of the Fermilab energy regime.

V Acknowledgment

We would like to thank A. Krzywicki for helpful correspondence.

TABLE I

Zone Structure Parameters

ALL ZONES	102 GeV/c		400 GeV/c	
	DATA	RCM	DATA	RCM
$\langle N_z \rangle$	$3.23 \pm .02$	2.96	$4.00 \pm .03$	3.40
$[\langle N_z^2 \rangle - \langle N_z \rangle^2]^{1/2}$	$1.13 \pm .01$	1.06	$1.51 \pm .01$	1.39
$\langle n_z \rangle$	$2.55 \pm .02$	2.81	$2.75 \pm .03$	3.24
$\langle \lambda_z \rangle$	$0.97 \pm .01$	1.15	$1.00 \pm .01$	1.29

TABLE II

Zone Structure for Central and End Zones

END ZONES	102 GeV/c		400 GeV/c	
	DATA	RCM	DATA	RCM
$\langle n_z \rangle$	$2.62 \pm .02$	2.94	$2.71 \pm .03$	3.43
$\langle \lambda_z \rangle$	$1.10 \pm .02$	1.38	$1.24 \pm .02$	1.73

CENTRAL ZONES	102 GeV/c		400 GeV/c	
	DATA	RCM	DATA	RCM
$\langle n_z \rangle$	$2.51 \pm .02$	2.57	$2.77 \pm .03$	2.93
$\langle \lambda_z \rangle$	$0.75 \pm .01$	0.78	$0.76 \pm .01$	0.84
$[\langle \lambda_z^2 \rangle - \langle \lambda_z \rangle^2]^{1/2}$	$0.73 \pm .01$	0.78	$0.80 \pm .01$	0.91

TABLE III

Semi-inclusive Zone Structure Parameters

102 GeV/c n_c	ALL ZONES			CENTRAL ZONES			END ZONES		
	$\langle n_z \rangle$	$\langle \lambda_z \rangle$	$\langle n_z \rangle$	$\langle n_z \rangle$	$\langle \lambda_z \rangle$	$\langle n_z \rangle$	$\langle n_z \rangle$	$\langle \lambda_z \rangle$	$\langle n_z \rangle$
2	2.00 ± .01	0.85 ± .04	2.00 ± .01	0.98 ± .04	2.00 ± .01	0.85 ± .04	2.00 ± .01	0.85 ± .04	2.00 ± .01
4	2.24 ± .02	1.01 ± .03	2.00 ± .01	0.98 ± .04	2.32 ± .02	1.03 ± .03	2.32 ± .02	1.03 ± .03	2.32 ± .02
6	2.45 ± .03	1.02 ± .02	2.28 ± .03	0.91 ± .03	2.55 ± .03	1.09 ± .03	2.55 ± .03	1.09 ± .03	2.55 ± .03
8	2.72 ± .03	1.00 ± .02	2.52 ± .03	0.73 ± .02	2.90 ± .05	1.23 ± .03	2.90 ± .05	1.23 ± .03	2.90 ± .05
10	2.84 ± .05	0.88 ± .03	2.72 ± .08	0.62 ± .03	2.97 ± .09	1.17 ± .04	2.97 ± .09	1.17 ± .04	2.97 ± .09
12	3.25 ± .12	0.95 ± .06	2.78 ± .12	0.54 ± .05	3.79 ± .20	1.41 ± .07	3.79 ± .20	1.41 ± .07	3.79 ± .20
≥14	3.25 ± .15	0.78 ± .05	3.18 ± .20	0.46 ± .07	3.49 ± .30	1.27 ± .08	3.49 ± .30	1.27 ± .08	3.49 ± .30
400 GeV/c									
2	2.00 ± .01	0.78 ± .07	2.00 ± .01	0.78 ± .07	2.00 ± .01	0.78 ± .07	2.00 ± .01	0.78 ± .07	2.00 ± .01
4	2.17 ± .02	1.03 ± .04	2.00 ± .01	1.07 ± .05	2.24 ± .02	1.01 ± .04	2.24 ± .02	1.01 ± .04	2.24 ± .02
6	2.35 ± .02	1.13 ± .03	2.21 ± .03	1.01 ± .04	2.44 ± .03	1.22 ± .04	2.44 ± .03	1.22 ± .04	2.44 ± .03
8	2.59 ± .03	1.14 ± .03	2.46 ± .03	0.91 ± .03	2.72 ± .05	1.34 ± .04	2.72 ± .05	1.34 ± .04	2.72 ± .05
10	2.70 ± .05	0.98 ± .03	2.59 ± .05	0.74 ± .03	2.85 ± .08	1.27 ± .05	2.85 ± .08	1.27 ± .05	2.85 ± .08
12	2.92 ± .06	0.97 ± .03	2.88 ± .08	0.74 ± .03	2.98 ± .10	1.29 ± .05	2.98 ± .10	1.29 ± .05	2.98 ± .10
14	3.14 ± .09	0.96 ± .04	2.99 ± .09	0.63 ± .03	3.37 ± .20	1.46 ± .07	3.37 ± .20	1.46 ± .07	3.37 ± .20
16	3.17 ± .10	0.88 ± .05	3.17 ± .15	0.60 ± .04	3.17 ± .20	1.40 ± .09	3.17 ± .20	1.40 ± .09	3.17 ± .20
18	3.33 ± .16	0.85 ± .07	3.31 ± .20	0.53 ± .05	3.39 ± .30	1.49 ± .10	3.39 ± .30	1.49 ± .10	3.39 ± .30
>20	3.83 ± .30	0.83 ± .08	3.93 ± .30	0.53 ± .06	3.14 ± .40	1.47 ± .10	3.14 ± .40	1.47 ± .10	3.14 ± .40

TABLE IV

Charge Transfer Averages

n_c	ℓ^-	r^-	102 GeV/c		400 GeV/c	
			$\langle u_{\ell^-, r^-} \rangle$	$\langle u_{\ell^-, r^-}^2 \rangle - \langle u_{\ell^-, r^-} \rangle^2$	$\langle u_{\ell^-, r^-} \rangle$	$\langle u_{\ell^-, r^-}^2 \rangle - \langle u_{\ell^-, r^-} \rangle^2$
2	0	0	$-.02 \pm .02$	$.17 \pm .02$	$-.01 \pm .03$	$.09 \pm .02$
4	1	0	$.24 \pm .02$	$.41 \pm .02$	$.26 \pm .03$	$.31 \pm .03$
6	2	0	$.62 \pm .04$	$.62 \pm .04$	$.49 \pm .05$	$.53 \pm .05$
	1	1	$.09 \pm .04$	$.62 \pm .04$	$.07 \pm .05$	$.52 \pm .05$
8	3	0	$1.15 \pm .08$	$.89 \pm .10$	$.92 \pm .08$	$.91 \pm .09$
	2	1	$.36 \pm .05$	$.86 \pm .06$	$.23 \pm .05$	$.82 \pm .06$
10	4	0	$1.3 \pm .2$	$1.6 \pm .6$	$1.0 \pm .2$	$1.1 \pm .2$
	3	1	$.87 \pm .11$	$1.1 \pm .2$	$.44 \pm .09$	$.90 \pm .10$
	2	2	$.18 \pm .09$	$.79 \pm .10$	$.03 \pm .11$	$1.10 \pm .16$
12	5	0	$2.3 \pm .3$	$.90 \pm .35$	$1.2 \pm .3$	$1.3 \pm .5$
	4	1	$1.0 \pm .3$	$1.2 \pm .3$	$1.05 \pm .14$	$1.14 \pm .22$
	3	2	$.39 \pm .14$	$1.2 \pm .2$	$.12 \pm .10$	$1.04 \pm .14$
14	6	0			$1.6 \pm .4$	$1.3 \pm .4$
	5	1	$1.5 \pm .4$	$1.1 \pm .4$	$1.1 \pm .2$	$.75 \pm .20$
	4	2	$0.8 \pm .4$	$1.7 \pm .9$	$.65 \pm .15$	$1.3 \pm .2$
	3	3	$0.3 \pm .4$	$0.9 \pm .6$	$-.14 \pm .20$	$1.4 \pm .3$
	7	0				
16	6	1				
	5	2			$.74 \pm .23$	$0.98 \pm .32$
	4	3	$0.1 \pm .5$	$2.1 \pm .8$	$-.12 \pm .20$	$1.7 \pm .4$
	7	1				
	6	2			$2.1 \pm .3$	$1.0 \pm .4$
18	5	3			$.23 \pm .36$	$1.6 \pm .9$
	4	4			$.00 \pm .4$	$2.4 \pm .9$
	7	1				
	6	2				

References and Footnotes

1. T. T. Chou and C. N. Yang, Phys. Rev. D7, 1425 (1973).
2. C. Quigg and G. H. Thomas, Phys. Rev. D7, 2752 (1973).
3. D. Sivers and G. H. Thomas, Phys. Rev. D9, 208 (1974).
4. A. Krzywicki and D. Weingarten, Phys. Letters 50B, 265 (1974).
5. D. Weingarten, Rochester preprint UR-505.
6. A. Krzywicki, Orsay preprint LPTHE 74/29.
7. C. Bromberg et al., Phys. Rev. D9, 1864 (1974).
8. For an examination of pp data at 69 GeV/c in terms of the LCC hypothesis, see J. Derré et al., French-Soviet Collaboration preprint M12 (1974).
9. The size of the bias can be gauged by the small positive values for $\langle u \rangle$, $0.07 \pm .02$ at 102 GeV/c and $0.03 \pm .03$ at 400 GeV/c; both numbers are consistent with estimates for the effects of proton contamination near $y=0$. See also Ref. 7.
10. C. Bromberg et al., Phys. Rev. Lett. 31, 1563 (1973); 32, 83 (1974).
11. The diagonal part of $D(y_1, y_2)$ is identical to a function defined by R. Baier and F.W. Bopp in a discussion of a neutral cluster model (University of Bielefeld preprint BI 74/06, 1974).
12. For completely uncorrelated charged particle production, $D(0,0)$ is given by $n_c/4$, consistent with the results of our RCM simulation.
13. References for the data in Fig. 5 are: U. Idschok, et al., 1973, Max Planck Inst. Rep. MPI-PAE/Exp. E1.29 (12,24 GeV/c); J. Derré et al., Ref. 8 (69 GeV/c); M. Pratap, private communication (205 GeV/c).
14. The MSU data are from Ref. 1 and private communication, B.Y. Oh.

Figure Captions

1. Zone graphs for two typical events; (a) An 8 prong at 102 GeV/c, (b) A 10 prong at 400 GeV/c. The graph is drawn with positive charges as upward-pointing arrows (\uparrow) and negative charges as downward-pointing arrows (\downarrow). The end zones, which contain the beam, (y_b), and target, (y_t), rapidities entering as negative (\downarrow) charges, are shaded.
2. Probability distributions for the number of zones per event.
3. Distributions in zone lengths.
4. The correlation function $D(y_1, y_2)$ evaluated at $y_1=0$, and $y_1=-1.2$, as a function of Δy . The curves are the results of randomizing the charge distributions in each event (RCM model described in the text).
5. Energy dependence of $\langle u^2 \rangle$.
6. (a) The mean of the charge transfer for fixed ℓ^- and r^- as a function of the difference ($\ell^- - r^-$). (b) The variance of the charge transfer for fixed ℓ^- and r^- as a function of the sum ($\ell^- + r^-$). Expectations for models with independent emission of single pions (Refs.1,2) are given as dashed lines.
7. Energy dependence of the mean charge transfer for fixed ℓ^- where $r^-=0$. The $(\ln s)^{-1}$ dependence expected in the cluster model are shown as straight lines passing through the origin.

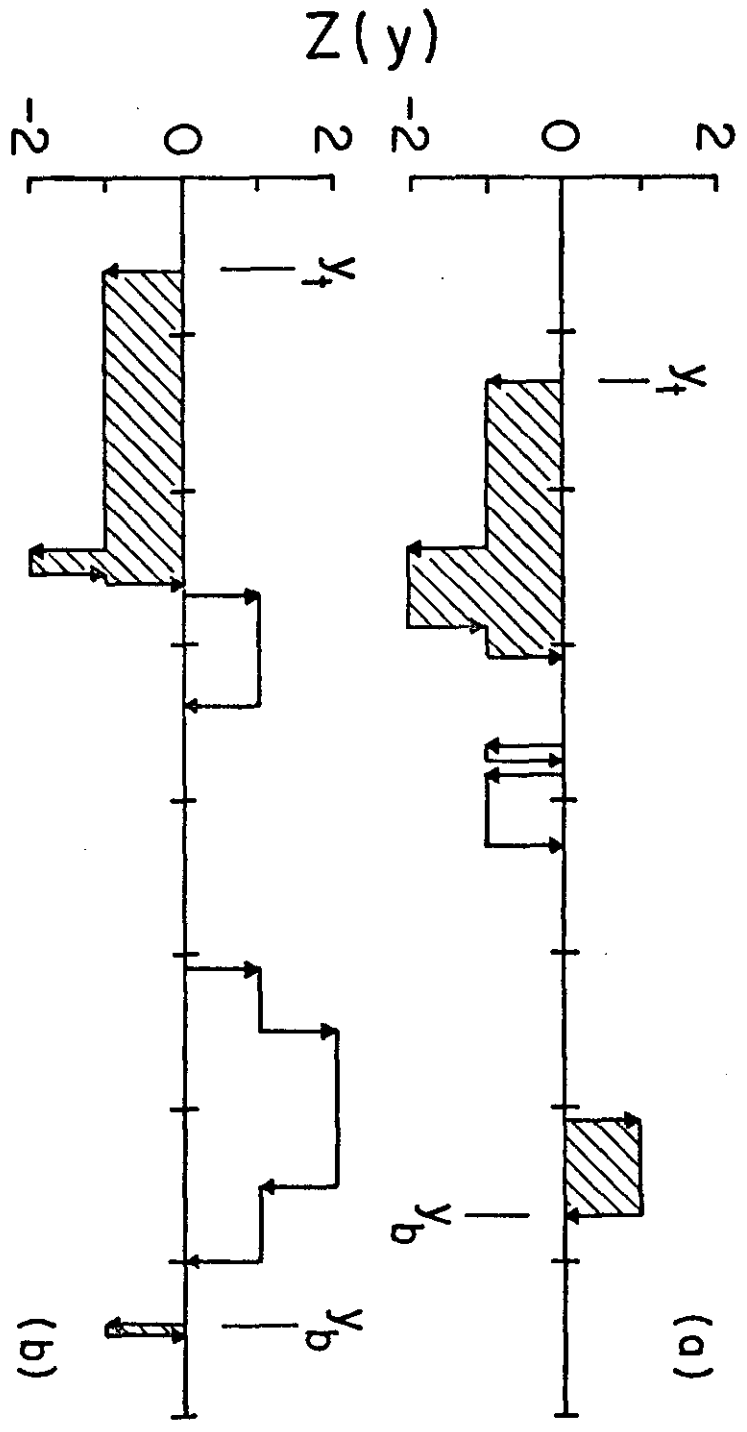


Fig 1

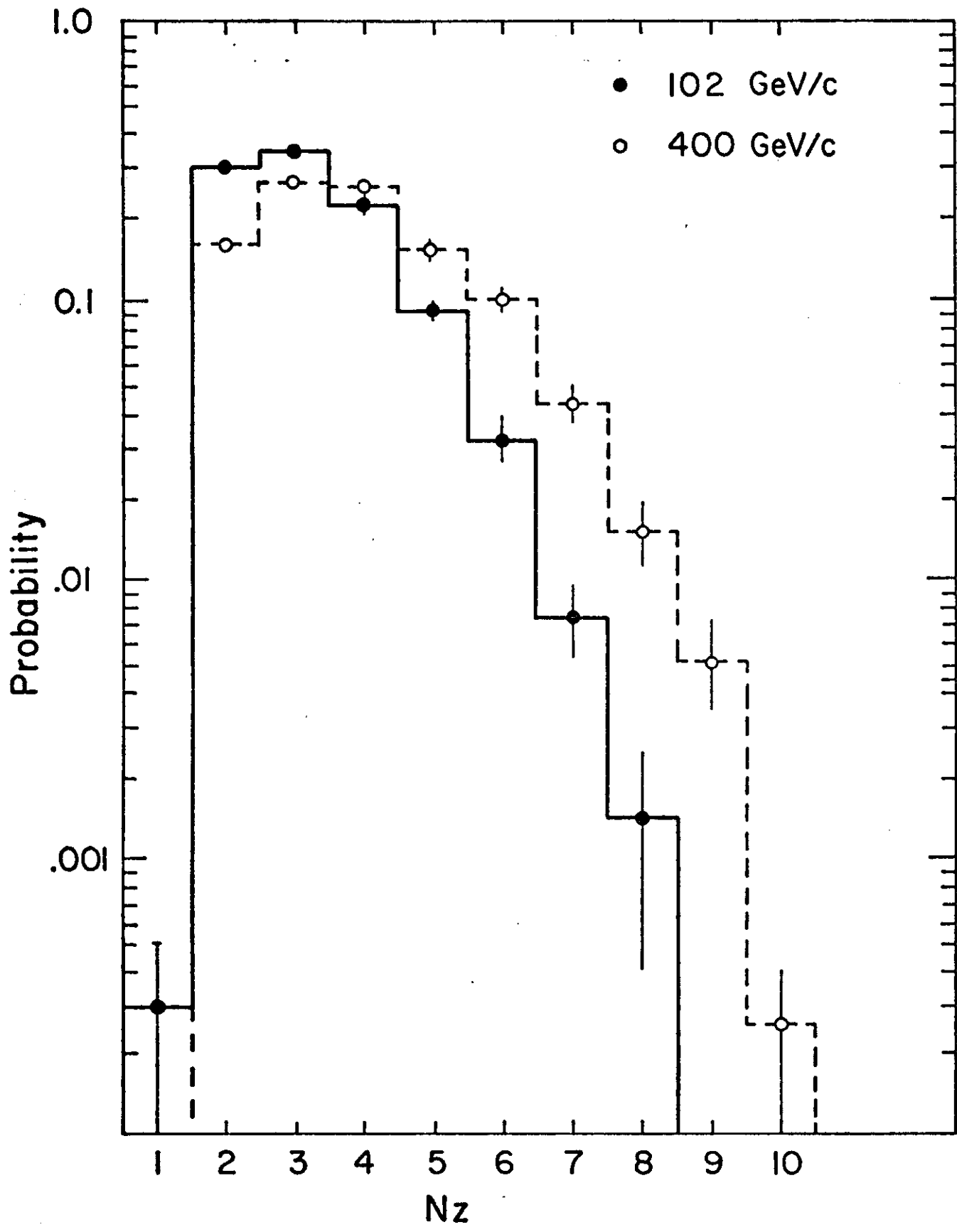
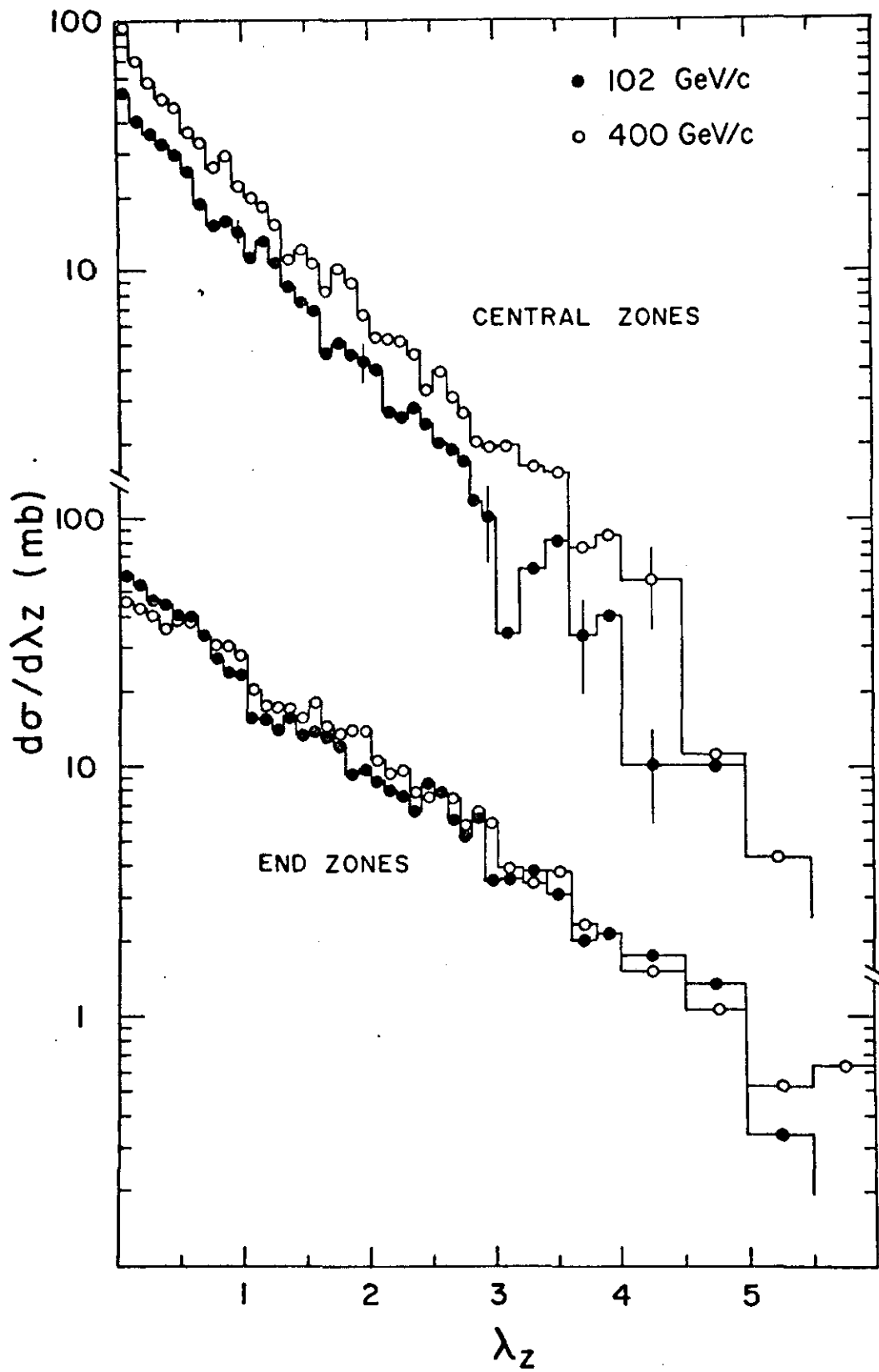


Fig 2



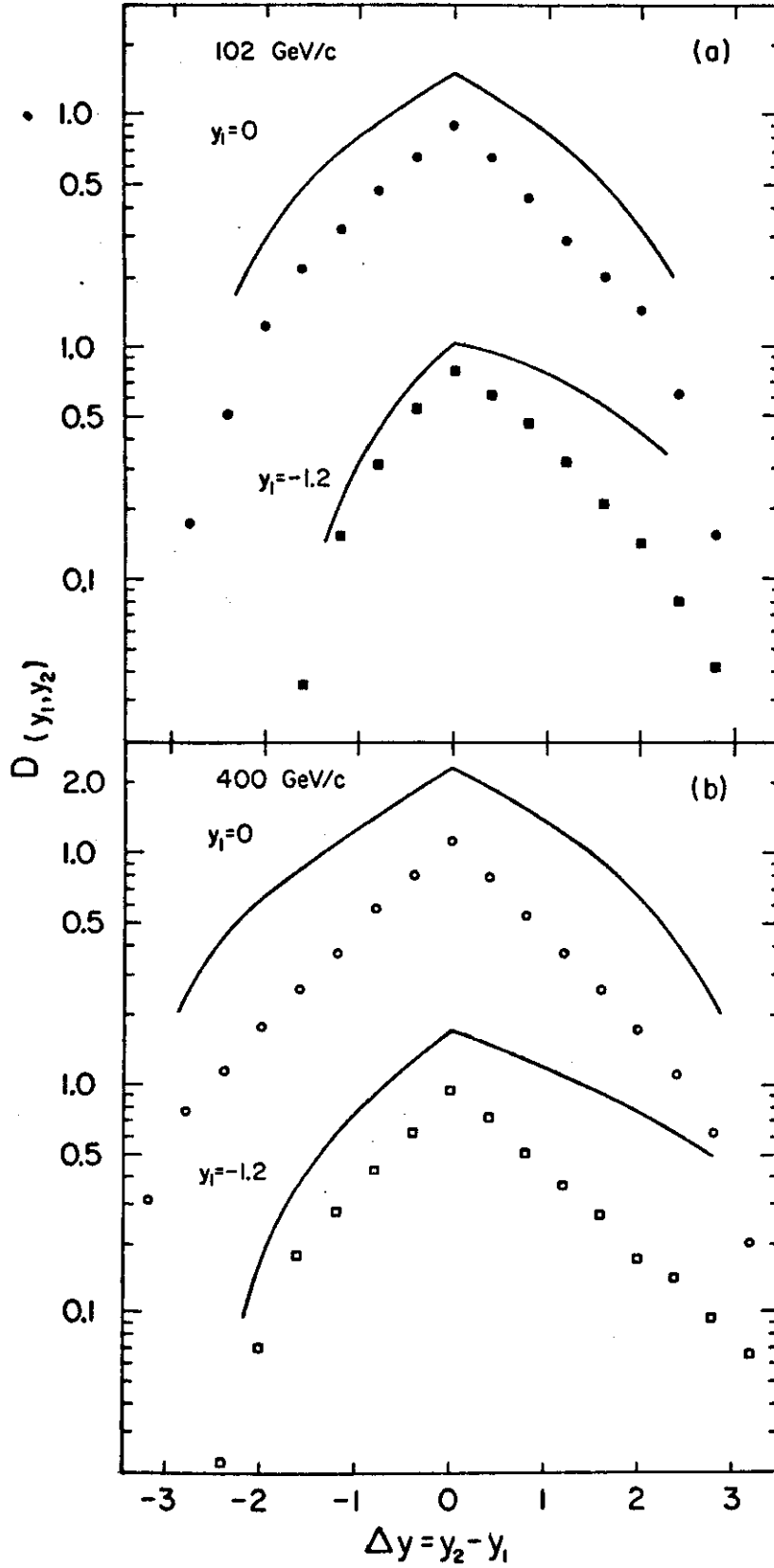


Fig 4

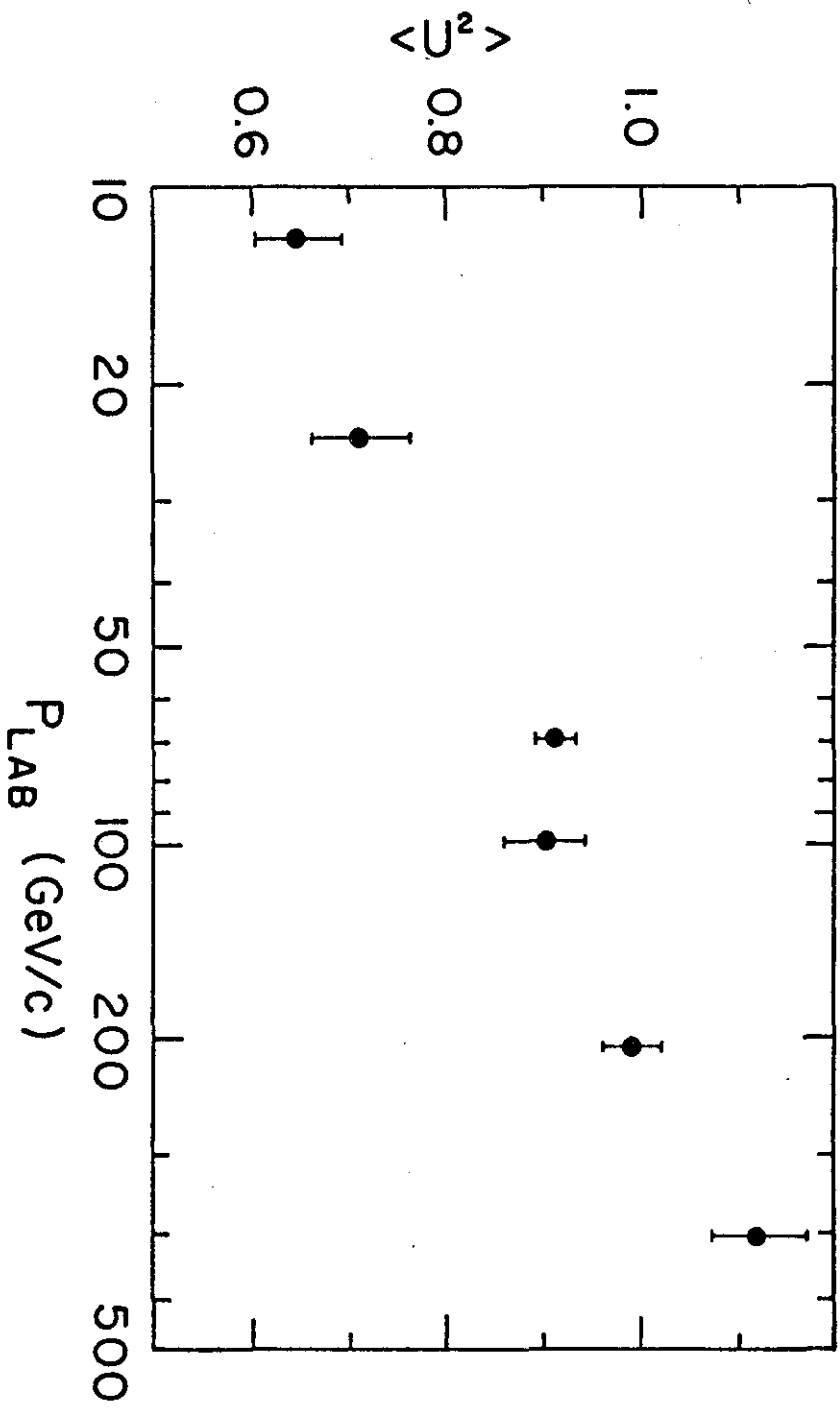
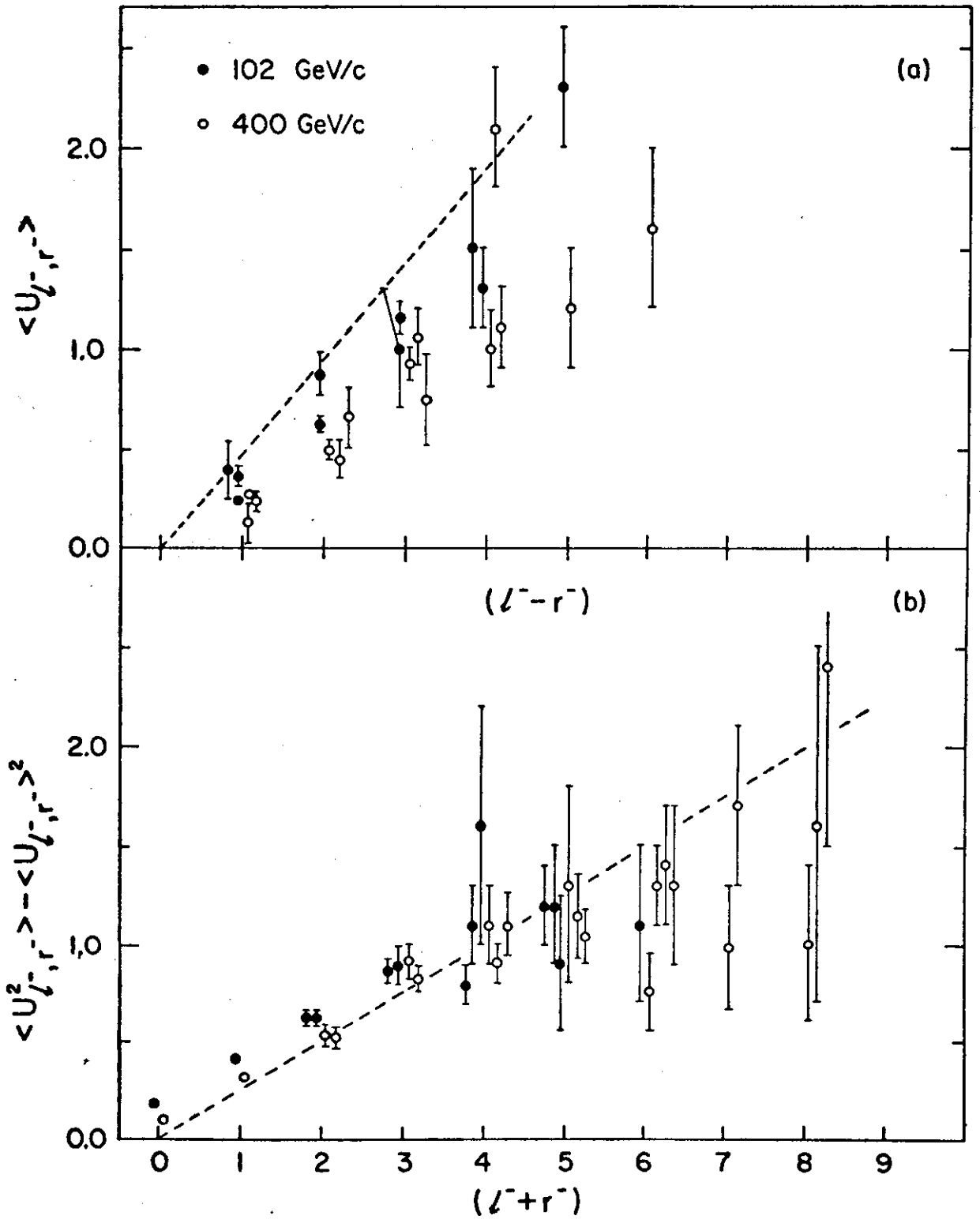


Fig 5



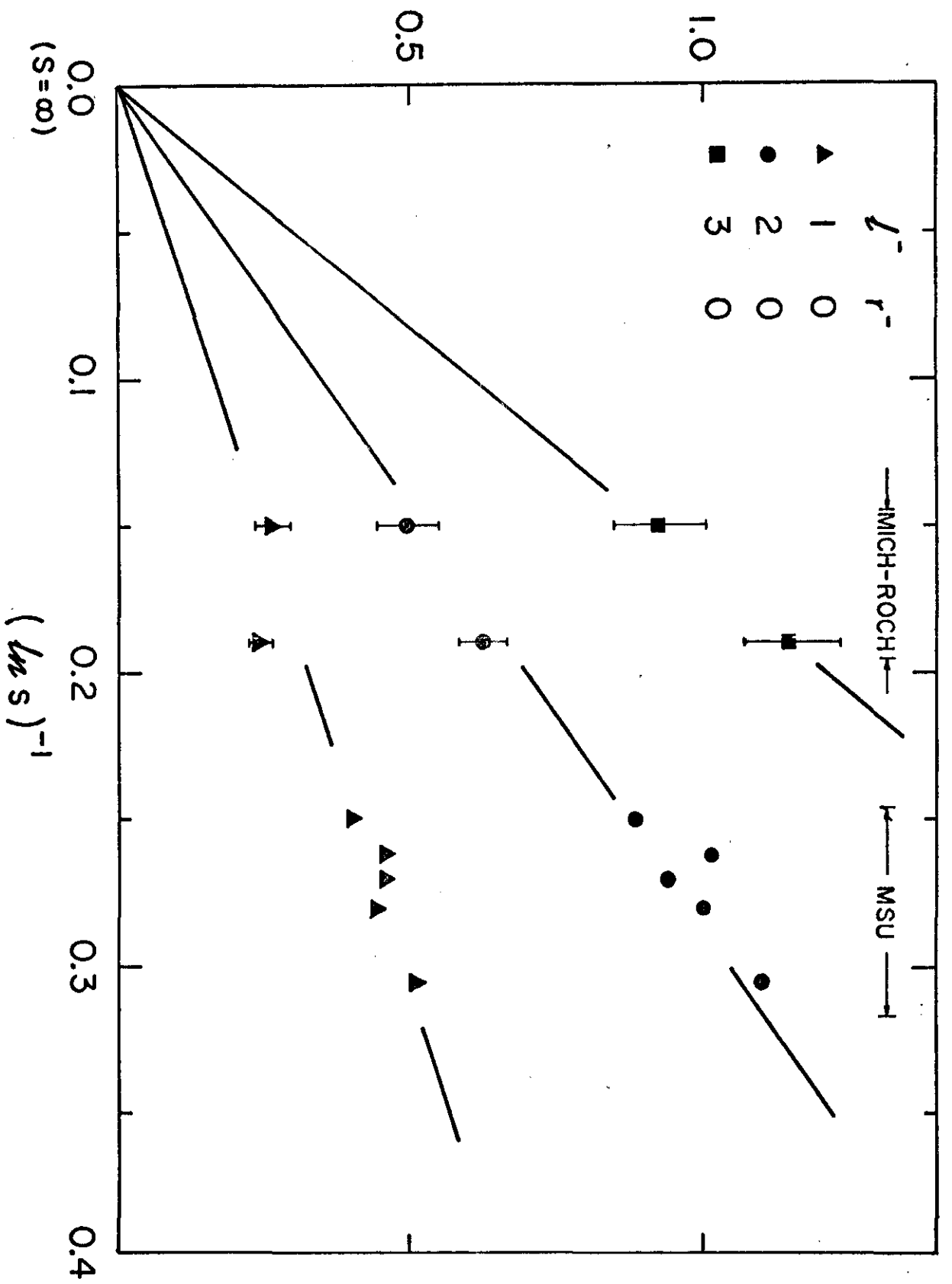


Fig 7